HHS Public Access

Author manuscript

J Bone Miner Res. Author manuscript; available in PMC 2017 January 19.

Published in final edited form as:

J Bone Miner Res. 2014 November ; 29(11): 2369–2381. doi:10.1002/jbmr.2281.

Ablation of Osteopontin Improves the Skeletal Phenotype of Phospho1−/− Mice

Manisha C Yadav[1], **Carmen Huesa**[2], **Sonoko Narisawa**[1], **Marc F Hoylaerts**[3], **Alain Moreau**[4], **Colin Farquharson**[2], and **José Luis Millán**[1]

[1]Sanford Children's Health Research Center, Sanford-Burnham Medical Research Institute, La Jolla, CA, USA

[2]The Roslin Institute and R(D)SVS, University of Edinburgh, Easter Bush, Midlothian, Scotland, UK

[3]Department of Cardiovascular Sciences, Center for Molecular and Vascular Biology, University of Leuven, Leuven, Belgium

[4]Department of Stomatology, Faculty of Dentistry, Department of Biochemistry, Faculty of Medicine, Université de Montréal, CHU Sainte-Justine Research Center, Montreal, Canada

Abstract

PHOSPHO1 and tissue-nonspecific alkaline phosphatase (TNAP) have nonredundant functions during skeletal mineralization. Although TNAP deficiency (*Alpl*$^{-/-}$ mice) leads to hypophosphatasia, caused by accumulation of the mineralization inhibitor inorganic pyrophosphate (PP_i), comparably elevated levels of PP_i in *Phospho1*$^{-/-}$ mice do not explain their stunted growth, spontaneous fractures, bowed long bones, osteomalacia, and scoliosis. We have previously shown that elevated PP_i in *Alpl*$^{-/-}$ mice is accompanied by elevated osteopontin (OPN), another potent mineralization inhibitor, and that the amount of OPN correlates with the severity of hypophosphatasia in mice. Here we demonstrate that plasma OPN is elevated and OPN expression is upregulated in the skeleton, particularly in the vertebrae, of *Phospho1*$^{-/-}$ mice. Liquid chromatography/tandem mass spectrometry showed an increased proportion of phosphorylated OPN (p-OPN) peptides in *Phospho1*$^{-/-}$ mice, suggesting that accumulation of p-OPN causes the skeletal abnormalities in *Phospho1*$^{-/-}$ mice. We also show that ablation of the OPN gene, *Spp1*, leads to improvements in the skeletal phenotype in *Phospho1*$^{-/-}$ as they age. In particular, their scoliosis is ameliorated at 1 month of age and is completely rescued at 3 months of age. There is also improvement in the long bone defects characteristic of *Phospho1*$^{-/-}$ mice at 3 months of age. Mineralization assays comparing [*Phospho1*$^{-/-}$; *Spp1*$^{-/-}$], *Phospho1*$^{-/-}$, and *Spp1*$^{-/-}$ chondrocytes display corrected mineralization by the double knockout cells. Expression of chondrocyte

Address correspondence to: José Luis Millán, PhD, Sanford-Burnham Medical Research Institute, 10901 North Torrey Pines Road, La Jolla, CA 92037, USA. millan@sanfordburnham.org.

Additional Supporting Information may be found in the online version of this article.

Disclosures

All authors state that they have no conflicts of interest.

Authors' roles: Study design: MCY, MFH, CF, and JLM. Study conduct: MCY, CH, SN, and MFH. Data collection: MCY, CH, and SN. Data analysis: MCY, CH, JLM, CF, and MFH. Data interpretation: MCY, JLM, CF, AM, and MFH. Drafting manuscript: MCY, CH, and JLM. JLM takes responsibility for the integrity of the data analysis.

differentiation markers was also normalized in the [*Phospho1*$^{-/-}$; *Spp1*$^{-/-}$] mice. Thus, although *Alpl* and *Phospho1* deficiencies lead to similar skeletal phenotypes and comparable changes in the expression levels of PP_i and OPN, there is a clear dissociation in the hierarchical roles of these potent inhibitors of mineralization, with elevated PP_i and elevated p-OPN levels causing the respective skeletal phenotypes in *Alpl*$^{-/-}$ and *Phospho1*$^{-/-}$ mice.

Introduction

PHOSPHO1 is active in the cytosol of osteoblasts and chondrocytes, as well as in their derived matrix vesicles (MVs), where it participates in MV-mediated calcification. [1, 2] Our recent studies have shown that PHOSPHO1 and tissue-nonspecific alkaline phosphatase (TNAP) play nonredundant functional roles in skeletal and dental mineralization. [3–5] PHOSPHO1 participates in the initiation of hydroxyapatite (HA) deposition inside MVs by scavenging P_i from phosphoethanolamine and phosphocholine, the head groups of the major phospholipids that constitute the plasma membrane of MVs, whereas TNAP facilitates propagation of HA crystals outside the MVs by restricting the concentrations of inorganic pyrophosphate (PP_i), a potent calcification inhibitor. [3–5] Remarkably, the double ablation of the PHOSPHO1 and TNAP function leads to the complete absence of skeletal and dental mineralization in mice. [3, 6]

Lack of murine PHOSPHO1 causes slow growth and skeletal deformities that include low bone mineral density, spontaneous greenstick fractures, osteomalacia, and prominent scoliosis. [3, 4] Both levoscoliosis and dextroscoliosis are observed in *Phospho1*$^{-/-}$ mice, but micro–computed tomography (μCT) ruled out the presence of any obvious morphological abnormalities, such as hemivertebrae or fused vertebrae. [3] Biochemically, *Phospho1*$^{-/-}$ mice show elevated levels of plasma PP_i, a change that is also observed in mice deficient in TNAP (*Alpl*$^{-/-}$), which manifest the soft bones disease known as hypophosphatasia (HPP). Indeed, correcting PP_i levels in *Alpl*$^{-/-}$ mice, either via cross-breeding *Alpl*$^{-/-}$ mice to a transgenic strain expressing human TNAP under control of the *ApoE* promoter, [*Alpl*$^{-/-}$*; ApoE-ALPL*], [7] or via enzyme-replacement therapy with a mineral-targeting recombinant form of TNAP [8] completely prevents the development of the skeletal and dental abnormalities characteristic of this mouse model of infantile HPP. However, reducing the PP_i levels in *Phospho1*$^{-/-}$ mice by cross-breeding them to the same *ApoE-ALPL* transgenic mice did not significantly improve the skeletal phenotype of *Phospho1*$^{-/-}$ mice. [3]

Osteopontin (OPN, encoded by *Spp1*) is another potent inhibitor of mineralization that is highly expressed in osteoblasts, as well as in osteoclasts. [9–12] OPN is an Arg-Gly-Asp motifcontaining matricellular protein [13] that contains several putative phosphorylation sites [14] and that can inhibit hydroxyapayite deposition in vitro when phosphorylated. [9] Furthermore, phosphorylation-dependent inhibition of mineralization by OPN appears to be mediated by ASARM peptides released from OPN by phosphate-regulating endopeptidase homolog, X-linked (PHEX) cleavage. [15] *Spp1*$^{-/-}$ mice have a skeleton that is histologically similar to wild-type (WT) mice and that is normal, even slightly hypermineralized. [16, 17] OPN expression is regulated by extracellular concentrations of

PP_i;[18–20] indeed, there is a linear correlation between PP_i and OPN concentrations in mutant mouse strains displaying dysregulation of PP_i metabolism, such as *Alpl*$^{-/-}$, *Enpp1*$^{-/-}$, and *ank/ank* mice. [17] However, ablating *Spp1* in an *Alpl* null background only partially rescued the HPP phenotype, confirming that the elevated PP_i concentrations caused HPP and that OPN only contributed partially to this phenotype. [17]

Given the increased levels of plasma PP_i observed in *Phospho1*$^{-/-}$ mice, we surmised that OPN levels would also be elevated in this mutant strain and that elevated OPN concentrations might contribute to the skeletal defects in this model of skeletal dysplasia. Remarkably, as shown in the present study, ablating *Spp1* function prevents the development of the skeletal phenotype of *Phospho1*$^{-/-}$ mice, establishing a primary role for OPN, rather than PP_i, in the pathophysiology of the *Phospho1*$^{-/-}$ skeletal defects.

Materials and Methods

Mice

Phospho1-R74X null mutant (*Phospho1*$^{-/-}$) mice were generated by N-ethyl-N-nitrosourea mutagenesis in a C3HeB/FeJ (Stock No. 000658, Jackson Laboratories, Bar Harbor, ME, USA) background, then bred to C57BL/6 mice to segregate other possible undesired mutations. [3] *Spp1*$^{-/-}$ mice were generated in a C57BL/6 background. [21] Founder *Spp1*$^{-/-}$ mice were imported from Japan (kindly provided by Prof. Masaki Noda) and re-derived into C57BL/6 mice. The resulting progeny were bred to obtain *Spp1*$^{+/-}$ mice, and the colony was maintained by heterozygote breeding. To generate mice lacking both PHOSPHO1 and OPN, *Phospho1*$^{-/-}$ mice were crossed to *Spp1*$^{-/-}$ mice, and double heterozygote mice were used to generate [*Phospho1*$^{-/-}$; *Spp1*$^{-/-}$] mice. The *Phospho1*$^{-/-}$ genotypes were determined using genomic DNA, PCR, and restriction digestion by *Bst*DI, and *Spp1*$^{-/-}$ genotypes were determined using genomic DNA and PCR protocols. [3, 18] The primer sequences for *Phospho1* genotyping were: sense 5′-TCCTCCTCACCTTCGACTTC-3′, antisense 5′-ATGCGGCGGAATAAACTGT-3′. Primer sequences for *Spp1* genotyping were: sense 5′-AGAGGTGAGGTCCTCATCTGTGGCA-3′ and antisense 5′-ACTCCAATCGTCCCTACAGTCGATGTC-3′. All animal procedures were reviewed and approved by our Institutional Animal Review Committee (Animal Use Form #12-114, Approval Date: 10/19/12).

Tissue and plasma collection, histological studies, and biochemical assays

Mice were euthanized by intraperitoneal injection of tribromoethanol, and blood was collected by cardiac puncture. Whole-body, long bone, and spine radiographic images were taken using an MX20 Specimen Radiograph System (Faxitron X-ray Corporation, Chicago, IL, USA) at 1 and 3 months of age. The lumbar spines, tibias, and femurs of 1-month- and 3-month-old mice were fixed in PBS containing 4% (w/v) paraformaldehyde. Plastic sections were stained with Von Kossa/van Gieson stain using published procedures, [7, 8, 22] and these sections were used to quantify osteoid volume using Bioquant Osteo Software (Bioquant Osteoanalysis Co., Nashville, TN, USA).

For OPN immunohistochemistry, bone tissues were decalcified with 0.125 M EDTA/10% formalin in H_2O (pH 7.2) for 5 days after fixation, and processed for paraffin sectioning. Immunostaining for OPN was performed using a goat anti-mouse-OPN antibody (Abcam, Cambridge, MA, USA) and a standard avidin-biotin complex protocol, using the Vectastain ABC Kit (Vector Laboratories, Burlingame, CA, USA).

Blood was collected by cardiac puncture and transferred into lithium heparin tubes. Plasma was separated by centrifugation at 5000 rpm for 10 minutes. Alkaline phosphatase activity and PP_i concentrations in plasma were measured using previously reported methods. [8] For PP_i assay, plasma was heated at 65°C for 10 minutes, 10 μL of plasma was diluted 4 times, and PP_i was measured by differential adsorption on activated charcoal of UDP-D-[6-3H]glucose (Amersham Pharmacia, Piscataway, NJ, USA), as previously described. [18, 23] This method uses a high specific activity UDP-D-[6-3H] glucose, which is separated from the reaction product 6-phospho-[6-3H] gluconate by selective adsorption on charcoal activated with phosphoric acid. Serial dilutions of sodium pyrophosphate (Sigma, St. Louis, MO, USA) are used as standards. Briefly, the diluted plasma samples and the standards are incubated at 37°C for 30 minutes in a reaction mixture containing NADP (Roche, Indianapolis, IN, USA), glucose-1,6-bisphosphate (Roche), uridine-5-(Roche), glucose-6 phosphate dehydrogenase (Roche), phosphoglucomutase (Sigma), uridine 5'-diphosphoglucose pyrophosphorylase (Sigma), and ^3H uridine dishposphoglucose (Amersham Pharmacia). The samples are then added to activated charcoal (Sigma). Each sample is run in duplicate or triplicate. After adsorption of the reaction mixture on charcoal, the sample is centrifuged at 13,000 rpm for 10 minutes, and a 100-μL aliquot of the supernatant carefully removed and assayed for radioactivity in 5 mL of Ecolume (MP Biomedicals, LLC, Solon, OH, USA). Mouse OPN was measured in plasma by ELISA (Enzo, Plymouth Meeting, PA, USA), following the manufacturer's protocol.

Micro–computed tomography (μCT)

Mice were euthanized at 1 and 3 months of age, as above, and the tibias and femurs were dissected and stored in water at −20°C. μCT analysis of the trabecular bone was performed on a 2-mm section of the right tibial and femoral metaphyses, 250 μm distal to the growth plate, using a Skyscan 1172 instrument (Kontich, Belgium) set at 60 kV, 150 μA, and a resolution of 5 μm. Cortical analysis was conducted on a 250-μm section located 2.25 mm distal to the reference growth plate. The spines were dissected from the cervical to the second lumbar vertebrae, and the thoracic vertebrae were scanned at a resolution of 20 μm. The images were reconstructed using the Skyscan NRecon program, analyzed using Skyscan CTAn, and the 3D models were visualized in Skyscan CTvol software. [3]

Mineralization assay and gene expression analysis

Primary chondrocytes were isolated from the knee joint growth plates of 5-day-old pups by collagenase digestion, as described previously. [3] Mineralization assays were performed by growing the cells in the presence of 2.5 mM β-glycerolphosphate and 50 mM ascorbic acid for 21 days and then staining with Alizarin red using a standard method. [18] RNA was extracted using an RNAeasy Plus Kit (Qiagen, Valencia, CA, USA). Specific RNA transcripts (mRNA) for *Alpl*, *Enpp1*, *Col2a1*, *Col10a1*, *Nr4a2*, *Mmp13*, *Phospho1*, and *Acan*

were quantified by real-time PCR using dual-labeled hydrolysis probes (FAM-TAMRA), as described previously. [3] Briefly, to carry out quantitative real-time PCR, 2 μL of the (1:10) diluted cDNA was used for assaying the amount of 18S endogenous ribosomal RNA and all the other genes of interest in duplicates. The reaction utilized 12.5 μL of platinum qPCR UDG Supermix (Invitrogen, Carlsbad, CA, USA), yielding 0.75 U Taq DNA polymerase, 20 mM Tris-HCl, 50 mM KCl, 3 mM MgCl2, and 200 μM of deoxynucleoside triphosphate. The reaction mixture was brought to a final concentration of 5 mM $MgCl_2$. Real-time reaction was performed in a 96-well plate on a Stratagene MX3000p real-time machine (Stratagene, La Jolla, CA, USA). Each assay was optimized by titrating a range of primer and probe concentrations and determining their cycle threshold (Ct) values. The primer and probe combinations that gave the lowest Ct and best amplification plots were used for the final analysis. Ct values were determined by the software according to the optimization of the baseline. For computing the relative amounts of all the genes, the average Ct of the primary signal for 18S was subtracted from that of gene of interest to give changes in Cts (dCt). A baseline dCt of 30 was subtracted and the results multiplied by – 1. In this manner, the degree of change in gene expression was determined. Relative units (a log2 scale dCt) were calculated and used here as a measure of gene expression. The normalization of all the genes with 18S controls for variation in the efficiency of RNA isolation, possible differences in amounts of starting RNA and RT efficiency.

Western blot and mass spectrometry analysis

After removal of skin, tendons, and muscle, leg and spine bones were snap-frozen with dry ice, and frozen bones were crushed into powder. The crushed bones and chondrocytes cultured for 21 days in mineralization media as described above were suspended in lysis solution (4 M guanidine HCl, 50 mM Tris HCl, 0.5 M EDTA, 2 mM phenylmethysulphonylfluoride, 5 mg/L pepstatin, and 1 mg/L soybean trypsin inhibitor; pH 7.5). [24] After rotation at 4°C for 48 hours, the samples were dialyzed against Tris-buffered saline solution containing 5 mM EDTA and 2 mM phenylmethysulphonylfluoride (pH 7.5) at 4°C to remove guanidine salt. Protein concentration was determined using a bicinchoninic acid assay kit according to manufacturer's instructions (Thermo Fisher Scientific Inc., Rockford, IL, USA). SDS-PAGE was performed as before. [25] OPN was detected using a goat anti-mouse-OPN antibody (Abcam, Cambridge, MA, USA) and the ECL Plus Kit (GE Healthcare, Pittsburgh, PA, USA).

For proteomic analysis, samples were prepared as previously described. [25] Briefly, guanidine/EDTA extracts of mineralized chondrocyte culture were incubated with a combination of mouse and goat anti-mouse OPN antibodies, and precipitated with Protein G agarose beads (Thermo Scientific, Carlsbad, CA, USA). Samples eluted from the Protein G beads were subjected to a TiO_2-based enrichment procedure. OPN phosphopeptides were analyzed by liquid chromatography and tandem mass spectrometry (LC-MS/MS) on a Michrom MS2 HPLC-captive spray-LTQ Orbitrap Velos with ETD instrument (Thermo Scientific) by the Proteomics core facility of the Sanford-Burnham Medical Research Institute (La Jolla, CA, USA).

OPN dephosphorylation by TNAP and PHOSPHO1, and phosphate-release assay

This assay was performed using a passive adsorption method on latex beads (Life Technologies, Carlsbad, CA, USA) according to the manufacturer's instructions. Briefly, latex beads were incubated with goat polyclonal antibody against mouse OPN (Abcam, Cambridge, MA, USA) overnight at 4°C. The beads were then washed and blocked with 1% (w/v) bovine serum albumin and incubated with plasma from WT mice, as a source of OPN. After washing, the beads were incubated with buffer as a negative control, recombinant TNAP (0.225 μM and 0.112 μM) and PHOSPHO1 (6.666 μM and 3.333 μM) and TNAP and PHOSPHO1 combined (0.112 μM TNAP and 3.333 μM PHOSPHO1) in separate reactions. The phosphate released into the supernatant was measured using the P_i ColorLock Gold phosphate detection system (Innova Biosciences, Cambridge, UK), according to the manufacturer's protocol, and absorbance was read at 630 nm. A phosphate (P_i) standard curve was generated, and readings taken at 5, 15, and 30 minutes of incubation showed a plateau in P_i concentration generated by TNAP at 30 minutes. Therefore, the reaction was monitored in the linear phase between 5 and 15 minutes, and the calibration line at 15 minutes was corrected for the baseline and used to convert $\Delta A_{630\ nm}$ over 10 minutes in P_i concentrations. Calibrations were then done taking the concentration of TNAP and PHOSPHO1 into account, and the apparent rate constants, expressed per second, were calculated.

Statistical analysis

All measurements were performed at least in triplicate. Results are expressed as mean ± standard error of the mean (SEM). The data were analyzed using Student's *t* test, and *p* values less than 0.050 were considered significant.

Results

Elevated osteopontin in the spine and plasma of *Phospho1*$^{-/-}$ mice

Immunohistochemistry demonstrated higher expression of OPN in the spine of 1-month-old *Phospho1*$^{-/-}$ mice than in the spine of WT littermate control mice (Fig. 1*A*), whereas no change in OPN expression was observed in their femurs (Fig. 1*B*). Significantly higher levels of OPN were also observed in the plasma of both 1- and 3-month-old *Phospho1*$^{-/-}$ mice than in WT mice (1-month-old, WT = 165.1 ± 11.21 ng/mL, *Phospho1*$^{-/-}$ = 203.9 ± 12.65 ng/mL, $p = 0.03$, $n = 11$; 3-months-old, WT = 94.90 ± 13.33 ng/mL, *Phospho1*$^{-/-}$ = 138.7 ± 13.55 ng/mL, $p = 0.03$, $n = 7$) (Fig. 1*C*). Similar results were found at the mRNA level, where quantitative real-time PCR showed that *Spp1* expression was 2.3-fold higher in the spine of *Phospho1*$^{-/-}$ mice than in WT mice (WT = 0.9240 ± 0.1314 [$n = 5$]; *Phospho1*$^{-/-}$ = 2.130 ± 0.4519 [$n = 4$], $p = 0.025$), whereas no differences were observed in the femur (WT = 1.635 ± 0.3323 [$n = 6$]; *Phospho1*$^{-/-}$ = 1.480 ± 0.2504 [$n = 5$], $p = 0.73$) (Fig. 1*D*). Because PP_i is known to affect *Spp1* expression, [18–20] we quantified the expression of *Enpp1* in the spine and legs and found higher *Enpp1* mRNA levels in the spine in all genotypes (Supplemental Fig. S1). Western blot analysis confirmed the higher expression of OPN in the spine of *Phospho1*$^{-/-}$ mice (Fig. 1*E*). Phosphopeptide sequences obtained from TiO_2-LC-MS/MS analysis of protein extracts of cultured chondrocytes from WT and *Phospho1*$^{-/-}$ mice immunoprecipitated with anti-OPN antibody (Fig. 1*F*) showed a

higher proportion of phosphorylated OPN (p-OPN) sequences in *Phospho1*$^{-/-}$ than in WT mice.

The aforementioned accumulation of p-OPN peptides could be because of lack of phosphatase activity of PHOSPHO1 or could be caused by the reduction in TNAP activity previously documented in *Phospho1*$^{-/-}$ mice. [3] To clarify this issue, we used passive adsorption of OPN onto latex beads and tested dephosphorylation by recombinant PHOSPHO1 and TNAP and then measured phosphate release by a colorimetric assay. The concentration of released P_i in the supernatants, using 0.22 μM TNAP and 6.66 μM PHOSPHO1, was 5.16 μM and 0.77 μM, respectively. The P_i release using both TNAP and PHOSPHO1 at half of the concentration of enzymes (0.112 μM and 3.33 μM for TNAP and PHOSPHO1, respectively) was only 0.97 μM. This shows that there is no synergy between both enzymes; the amount of phosphate release with both TNAP and PHOSPHO1 together essentially corresponds to the activity expected for TNAP alone. The mean apparent rate constants for antibody-bound OPN hydrolysis by TNAP and PHOSPHO1 were 3.4×10^{-2}/s and 8×10^{-5}/s, respectively. The ratio between the rate constants for both enzymes was 424, which shows that TNAP is about 400 times more active in OPN dephosphorylation than PHOSPHO1.

Rescue of the scoliosis phenotype and improvement at other skeletal sites in the *Phospho1*$^{-/-}$ mice by the deletion of *Spp1*

Ablation of OPN function in the *Phospho1*$^{-/-}$ background improved the spinal deformity characteristic of this skeletal dysplasia model. X-ray imaging showed that the scoliosis phenotype was considerably less pronounced in the [*Phospho1*$^{-/-}$; *Spp1*$^{-/-}$] mice than in *Phospho1*$^{-/-}$ mice at 1 month of age, and it was completely absent at 3 months of age. *Phospho1*$^{-/-}$ mice show severe long bone deformities such as bowed or deformed tibias and spontaneous fractures both in the femurs and tibias both at 1 and 3 months of age. Improvement in the long bone deformities was observed in [*Phospho1*$^{-/-}$; *Spp1*$^{-/-}$] mice at 3 months of age (Fig. 2*A*, *B*).

Histomorphometric analyses using Von Kossa/Van Gieson staining confirmed that the osteomalacia previously reported in 10-day-old *Phospho1*$^{-/-}$ mice [3] persisted at 1 month (Supplemental Fig. S2) and 3 months of age (Fig. 3, arrows). The vertebral sections also showed the presence of widespread hyperosteoidosis in the *Phospho1*$^{-/-}$ mice (Supplemental Fig. S2 and Fig. 3, arrows). The osteomalacia in the vertebrae and the long bones of [*Phospho1*$^{-/-}$; *Spp1*$^{-/-}$] mice was somewhat reduced at 1 month of age and significantly at 3 months of age compared with *Phospho1*$^{-/-}$ mice (Fig. 3 and Supplemental Fig. S2). The significance of the comparison of percentage osteoid volume to bone volume (OV/BV%) measured in the tibias at 1 month of age were: WT versus *Phospho1*$^{-/-}$, $p = 0.035$ ($n = 4$) and *Phospho1*$^{-/-}$ versus [*Phospho1*$^{-/-}$; *Spp1*$^{-/-}$], $p = 0.043$ ($n = 4$) and for vertebral OV/BV%, WT versus *Phospho1*$^{-/-}$, $p = 0.004$ ($n = 4$) and *Phospho1*$^{-/-}$ versus [*Phospho1*$^{-/-}$; *Spp1*$^{-/-}$], $p = 0.003$ ($n = 4$). Similarly, at 3 months of age, the significance for tibial OV/BV% differences were: WT versus *Phospho1*$^{-/-}$, $p = 0.009$ ($n = 4$) and *Phospho1*$^{-/-}$ versus [*Phospho1*$^{-/-}$; *Spp1*$^{-/-}$], $p = 0.02$ ($n = 4$) and for vertebral OV/BV%, WT versus *Phospho1*$^{-/-}$, $p = 0.0007$ ($n = 4$) and *Phospho1*$^{-/-}$ versus [*Phospho1*$^{-/-}$;

Spp1$^{-/-}$], $p = 0.0008$ ($n = 4$). Scoliosis was observed at 1 month, as shown before, [3] and 3 months (Fig. 4*A*) of age in the *Phospho1*$^{-/-}$ mice by μCT where the top thoracic vertebrae (T_2 to T_4) appear rotated in their axis. Scoliosis was observed in the [*Phospho1*$^{-/-}$; *Spp1*$^{-/-}$] mice at 1 month of age but not at 3 months of age (Fig. 4*A*).

At 1 month of age, trabecular analysis of the tibias and femurs of *Spp1*$^{-/-}$ mice showed parameters comparable to WT mice (Supplemental Tables S1 and S2). However, at 3 months of age, *Spp1*$^{-/-}$ mice showed significantly higher trabecular bone volume per selected area of tissue volume (%BV/TV) than WT mice in both femurs (WT = 11.58 ± 1.607, *Spp1*$^{-/-}$ = 25.23 ± 3.009, $p = 0.0035$) and tibias (WT = 9.697 ± 1.852, *Spp1*$^{-/-}$ = 19.32 ± 2.796, $p = 0.016$), which reflects the larger trabecular number and lower trabecular space measured (Fig. 4*B*, and Supplemental Tables S1 and S2). BV/TV was significantly higher in the tibias of [*Phospho1*$^{-/-}$; *Spp1*$^{-/-}$] mice compared with *Phospho1*$^{-/-}$ mice at 1 month of age ([*Phospho1*$^{-/-}$; *Spp1*$^{-/-}$] = 8.84 ± 0.62%, *Phospho1*$^{-/-}$ 6.75 ± 0.39%, $p = 0.02$) (Fig. 4*B* and Supplemental Table S1). Trabeculae in the tibias were significantly thicker at 1 month of age in the [*Phospho1*$^{-/-}$; *Spp1*$^{-/-}$] compared with *Phospho1*$^{-/-}$ mice ([*Phospho1*$^{-/-}$; *Spp1*$^{-/-}$] = 38.74 ± 0.67 μm, *Phospho1*$^{-/-}$ = 35.23 ± 1.09 μm, $p = 0.02$) (Fig. 4*C* and Supplemental Table S1), and larger trabecular number and lower trabecular space were also observed at 3 months of age in these mice (Supplemental Table S1). Cortical measurements of the tibias (Fig. 4*D* and Supplemental Table S3) showed higher cortical porosity in *Phospho1*$^{-/-}$ mice both at 1 and 3 months of age compared with WT mice (WT mice = 3.548 ± 0.364 versus *Phospho1*$^{-/-}$ mice = 9.543 ± 1.29, $p = 0.006$ at 1 month of age; WT mice = 1.343 ± 0.272 versus *Phospho1*$^{-/-}$ mice = 2.413 ± 0.399, $p = 0.032$ at 3 months of age). At this age, the [*Phospho1*$^{-/-}$; *Spp1*$^{-/-}$] double knockout tibias had a mean % cortical porosity value that was not statistically significant compared with that of the *Phospho1*$^{-/-}$ or WT tibia ([*Phospho1*$^{-/-}$; *Spp1*$^{-/-}$] mice = 6.957 ± 1.209 versus WT mice = 3.548 ± 0.364, $p = 0.10$; [*Phospho1*$^{-/-}$; *Spp1*$^{-/-}$] 6.957 ± 1.209 versus *Phospho1*$^{-/-}$ 9.543 ± 1.29, $p = 0.09$). Cortical thickness of the tibias was also significantly higher in [*Phospho1*$^{-/-}$; *Spp1*$^{-/-}$] mice than in *Phospho1*$^{-/-}$ mice at 1 month of age (WT = 168.7 ± 11.39 μm, *Phospho1*$^{-/-}$ = 142.2 ± 2.25 μm, WT versus *Phospho1*$^{-/-}$, $p = 0.02$, *Spp1*$^{-/-}$ = 172.0 ± 3.72 μm, [*Phospho1*$^{-/-}$; *Spp1*$^{-/-}$] = 157.2 ± 4.32 μm, *Phospho1*$^{-/-}$ versus [*Phospho1*$^{-/-}$; *Spp1*$^{-/-}$], $p = 0.01$) (Fig. 4*D*, *E*). Cortical bone mineral densities (BMD) (Fig. 5*A*, *B*) of both femurs and tibias of 1-month-old mice were lower in *Phospho1*$^{-/-}$ mice than in WT mice but were significantly higher in [*Phospho1*$^{-/-}$; *Spp1*$^{-/-}$] than in *Phospho1*$^{-/-}$ mice (WT = 1.21 ± 0.02 g/cm^3, *Phospho1*$^{-/-}$ = 1.09 ± 0.017 g/cm^3, WT versus *Phospho1*$^{-/-}$, $p = 0.003$, *Spp1*$^{-/-}$ = 1.23 ± 0.013 g/cm^3, [*Phospho1*$^{-/-}$; *Spp1*$^{-/-}$] = 1.17 ± 0.01 g/cm^3, *Phospho1*$^{-/-}$ versus [*Phospho1*$^{-/-}$; *Spp1*$^{-/-}$], $p = 0.006$) (Fig. 5*A*, *B*). No significant difference was observed between *Spp1*$^{-/-}$ and WT mice. The BMD of the tibias and femurs at 3 months of age did not show any significant differences between WT, *Phospho1*$^{-/-}$, and [*Phospho1*$^{-/-}$; *Spp1*$^{-/-}$] mice (Fig. 5*A*, *B*).

In vitro chondrocyte mineralization and plasma analysis

To check the mineralization ability of primary chondrocytes, cells from WT, *Phospho1*$^{-/-}$, *Spp1*$^{-/-}$, and [*Phospho1*$^{-/-}$; *Spp1*$^{-/-}$] mice were grown in culture for 14 and 21 days in the presence of mineralization medium containing ascorbic acid and β-glycerolphosphate. Similar results were obtained both at day 14 (data not shown) and day 21 of culture (Fig. 6).

Phospho1$^{-/-}$ *and Spp1*$^{-/-}$ cells showed lower mineralization than WT cells, whereas [*Phospho1*$^{-/-}$; *Spp1*$^{-/-}$] chondrocytes had significantly higher mineralization than *Phospho1*$^{-/-}$ cells (WT = 25.22 ± 5.46, *Phospho1*$^{-/-}$ = 14.29 ± 3.83, *Spp1*$^{-/-}$ = 7.22 ± 2.23, [*Phospho1*$^{-/-}$; *Spp1*$^{-/-}$] = 29.49 ± 1.82 mmols of bound alizarin red, *Phospho1*$^{-/-}$ versus [*Phospho1*$^{-/-}$; *Spp1*$^{-/-}$], $p = 0.023$) (Fig. 6*A*). Interestingly, *Phospho1* gene expression was significantly lower in the spine and leg, as well as primary chondrocytes, of *Spp1*$^{-/-}$ mice (spine, WT= 1.57 ± 0.38, *Spp1*$^{-/-}$ = 0.38 ± 0.06, $p = 0.03$; legs, WT = 1.07 ± 0.28, *Spp1*$^{-/-}$ = 0.08 ± 0.004, $p = 0.02$; 21-day cultured chondrocytes, WT = 2.68 ± 0.93, *Spp1*$^{-/-}$ = 0.73 ± 0.21, $p = 0.02$) (Fig. 6*B*). In addition, *Alpl* expression in chondrocytes from *Phospho1*$^{-/-}$ and *Spp1*$^{-/-}$ mice was approximately twofold lower than in chondrocytes from WT mice (Fig. 6*C*), whereas *Alpl* expression in chondrocytes from [*Phospho1*$^{-/-}$; *Spp1*$^{-/-}$] mice was comparable to WT. *Enpp1* expression was approximately threefold higher in chondrocytes from [*Phospho1*$^{-/-}$; *Spp1*$^{-/-}$] mice than in WT, *Phospho1*$^{-/-}$, and *Spp1*$^{-/-}$ cells (WT = 194,949 ± 33,283, *Phospho1*$^{-/-}$ = 104,565 ± 10,658, WT versus *Phospho1*$^{-/-}$, $p = 0.01$, *Spp1*$^{-/-}$ = 89,762 ± 21,227, [*Phospho1*$^{-/-}$; *Spp1*$^{-/-}$] = 219,266 ± 46,728, *Phospho1*$^{-/-}$ versus [*Phospho1*$^{-/-}$; *Spp1*$^{-/-}$], $p = 0.03$; WT versus [*Phospho1*$^{-/-}$; *Spp1*$^{-/-}$], $p = 0.71$) (Fig. 6*D*). Consistent with the gene expression data, *Phospho1*$^{-/-}$ mice had lower plasma TNAP activity than WT littermate control mice, whereas plasma TNAP activity was significantly higher in the [*Phospho1*$^{-/-}$; *Spp1*$^{-/-}$] compared with *Phospho1*$^{-/-}$ mice (*Phospho1*$^{-/-}$ = 272.2 ± 18.16 mmol/μL/min, [*Phospho1*$^{-/-}$; *Spp1*$^{-/-}$] = 400.1 ± 32.95 mmol/μL/min, $p = 0.007$) (Fig. 6*E*). As TNAP hydrolyzes the mineralization inhibitor PP_i, we determined plasma PP_i levels in 3-month-old mice. Consistent with the measured TNAP levels and our previous reports, [3, 17] we observed high PP_i levels in *Phospho1*$^{-/-}$ and *Spp1*$^{-/-}$ mice, whereas the [*Phospho1*$^{-/-}$; *Spp1*$^{-/-}$] mice showed normal PP_i levels (WT = 42.27 ± 2.005 μM, *Phospho1*$^{-/-}$ = 46.99 ± 0.9110 μM, *Spp1*$^{-/-}$ = 46.98 ± 1.73 μM [*Phospho1*$^{-/-}$; *Spp1*$^{-/-}$] = 40.92 ± 2.434 μM, WT versus *Phospho1*$^{-/-}$, $p = 0.03$; *Phospho1*$^{-/-}$ versus [*Phospho1*$^{-/-}$; *Spp1*$^{-/-}$], $p = 0.0093$; WT versus [*Phospho1*$^{-/-}$; *Spp1*$^{-/-}$], $p = 0.69$) (Fig. 6*F*). Because we had previously reported changes in chondrocyte gene expression in *Phospho1*$^{-/-}$ chondrocytes, [3] we next examined whether any genes might show a normal pattern of expression in the [*Phospho1*$^{-/-}$; *Spp1*$^{-/-}$] cells. Expression of the chondrocyte differentiation markers *Nr4a2, Col2a1*, *Acan*, *Col10a1*, and *Runx2* was lower in cells from *Phospho1*$^{-/-}$ mice than in [*Phospho1*$^{-/-}$; *Spp1*$^{-/-}$] cells. *Mmp13* expression was higher in chondrocytes from [*Phospho1*$^{-/-}$; *Spp1*$^{-/-}$] compared with WT, *Phospho1*$^{-/-}$, and *Spp1*$^{-/-}$ cells (Supplemental Fig. S3).

Discussion

We have previously shown that PHOSPHO1 has a nonredundant function in the initiation of calcification, as *Phospho1*$^{-/-}$ mice have spontaneous fractures, bowed long bones, osteomalacia, and scoliosis, [3] with approximately 30% to 40% of *Phospho1*$^{-/-}$ mice showing thoracic scoliosis on postnatal day 10, and 100% of them having the top thoracic vertebrae (T_2 to T_4) rotated in their own axis at 1 month of age. However, the skeletal abnormalities in *Phospho1*$^{-/-}$ mice could not be explained by increased levels of the mineralization inhibitor PP_i because normalizing PP_i concentrations did not prevent their skeletal phenotype. [3] Interestingly, Moreau and colleagues showed that high circulating

levels of OPN were associated with idiopathic scoliosis onset and spinal deformity progression. [26]

OPN is another potent inhibitor of mineralization. [16, 27–30] It is a matricellular protein that modulates cell-matrix interactions and cell function, [11] without having a structural role itself, [31] and is highly associated with mineralized tissue. [24] Although *Spp1*$^{-/-}$ mice are both histologically and radiographically normal, [32] there are reports that suggest that OPN has an inhibitory function in mineralization. [16, 27–30] Recently, we reported that OPN is a physiological substrate of TNAP, and identified at least two preferred sites of dephosphorylation by TNAP. [25] We also documented that the levels of plasma OPN correlated with the severity of the HPP phenotype in *Alpl*$^{-/-}$ mice. [25]

Given that PP_i induces OPN expression [17, 19, 20] and the strict positive correlation that we had found between PP_i and OPN plasma levels in various knockout mouse strains, [17] we tested the hypothesis that ablating OPN function would prevent the skeletal phenotype, particularly the scoliosis, in *Phospho1*$^{-/-}$ mice. Indeed, deletion of OPN on the *Phospho1*$^{-/-}$ background, [*Phospho1*$^{-/-}$; *Spp1*$^{-/-}$], prevented the scoliosis phenotype and, to some extent, the HPP-like osteomalacia phenotype of *Phospho1*$^{-/-}$ mice. The differential effect of this improvement is likely the result of the much higher levels of *Spp1* expressed in the axial versus the appendicular skeleton. In turn, our findings that *Enpp1* expression is also much higher in the axial compared with the appendicular skeleton suggests that local differences in the levels of PP_i may be responsible for the site-specific regulation of OPN expression. As we recently demonstrated that TNAP physiologically dephosphorylates OPN and affects the ability of OPN to inhibit mineralization, we further hypothesized that PHOSPHO1 can also act as a phosphatase and dephosphorylate OPN and this explains the improvement observed in the [*Phospho1*$^{-/-}$; *Spp1*$^{-/-}$] mice. This would also explain the greater proportion of phosphorylated OPN peptides observed in *Phospho1*$^{-/-}$ mice than in WT mice. However, we found that PHOSPHO1 dephosphorylates OPN inefficiently, suggesting that the reduction in TNAP activity previously documented in *Phospho1*$^{-/-}$ mice [3] causes the accumulation of p-OPN in this animal model. OPN triggers *Alpl* gene expression through αvβ3 integrin-mediated FAK activation, [33] so *Alpl* gene expression is reduced in the absence of OPN. Our findings that *Spp1*$^{-/-}$ vertebrae, long bones, and cultured chondrocytes also show low expression of *Phospho1*$^{-/-}$ adds *Phospho1* to the list of genes that are regulated by OPN, which already includes including *Alpl*, *Enpp1*, and *Ank*. [17]

Fig. 7 summarizes our current understanding of the complex counter-regulatory influence of the P_i/PP_i ratio, OPN, and now also PHOSPHO1 on mineralizing cells. Although PP_i has a major role in controlling deposition in the ECM, changes in the extracellular P_i/PP_i ratio, likely sensed by sodium-dependent phosphate transporters (P_iT1 and/or 2), [34] affect expression of the genes that control the levels of extracellular PP_i (*Enpp1, Ank, Alpl*), as well as OPN. In turn, OPN, especially as p-OPN, [16, 27–30] participates in controlling hydroxyapatite deposition in the ECM while also influencing the expression of *Enpp1*, *Ank*, and *Alpl*, [17] as well as *Phospho1*. PHOSPHO1 appears to control the expression of OPN, as well as the output of PP_i, thus acting as upstream regulator to both of these important counter-regulated inhibitory pathways.

Given the reduction in *Phospho1* expression shown here in *Spp1*$^{-/-}$ cells, we can interpret the reduction of TNAP activity in *Spp1*$^{-/-}$ mice as a combination of direct downregulation of the *Alpl* gene in the absence of OPN, as well as a downstream effect caused by the reduction in PHOSPHO1 expression caused by OPN deficiency. As indicated in our mass spectrometry data, the increased level of p-OPN peptides in *Phospho1*$^{-/-}$ mice is consistent with the expected hyperphosphorylation status of OPN caused by the very low levels of TNAP activity in these *Phospho1*$^{-/-}$ animals. Thus, it seems clear that the prominent scoliosis phenotype of *Phospho1*$^{-/-}$ mice may be caused by the increased levels of OPN in the spine caused by the higher levels of *Enpp1* expression in the spine and accumulation of p-OPN, owing to the sharp reduction in TNAP activity resulting from PHOSPHO1 deficiency. Thus, in the *Phospho1*$^{-/-}$ model, it is the accumulation of the mineralization inhibitor p-OPN that appears to cause the disease phenotype, rather than a build-up of PP_i. Indeed, we previously showed that *Phospho1*$^{-/-}$ mice overexpressing TNAP under control of the *ApoE* promoter had high levels of plasma TNAP and normal plasma PP_i but no significant correction of their skeletal phenotype. [3] In contrast, correcting plasma PP_i levels in *Alpl*$^{-/-}$ HPP mice prevented all the skeletal and dental manifestations of this model of osteomalacia. [8] Thus, we have two skeletal dysplasias that display similar biochemical changes—elevation of both PP_i and p-OPN concentrations—in which the hierarchical roles of these potent mineralization inhibitors appear to be different, with elevations in PP_i largely explaining the HPP phenotype and elevations of p-OPN largely explaining the *Phospho1*$^{-/-}$ phenotype. Why did the transgenic overexpression of TNAP in the liver not lead to improvement of the *Phospho1*$^{-/-}$ phenotype? We think that this has to do with the fact that soluble circulating TNAP does not reach cartilage very well, possibly because of vascularity issues. Previous attempts at enzyme-replacement therapy with plasma TNAP in the early 1980s failed to yield life-saving treatment to children affected by severe HPP. [35, 36] The interpretation of those data has been that TNAP is needed locally at sites of initiation of matrix vesicle–mediated mineralization in the growth plate and in bone. The efficacy demonstrated by the use of mineral-targeting TNAP in the treatment of mice [8] and humans [37] with life-threatening HPP is consistent with that premise. In addition, our recent data examining *Alpl*$^{-/-}$ mice bred to *ApoE-Tnap* or to *Col1a1-Tnap* transgenic mice expressing soluble TNAP showed that although PP_i was corrected in the plasma and the skeletal defect was improved, the animals still developed growth plate and joint abnormalities with age. [25] Those cartilage defects are not seen in mice treated with mineral-targeting TNAP. [8] We think that mineral-targeting TNAP is able to reach sites of impending mineralization in cartilage, whereas soluble TNAP is not. Thus, although the elevated levels of plasma TNAP achieved by the transgenic overexpression of TNAP in the liver is able to normalize plasma PP_i concentrations, we think that the enzyme does not reach sites of impending mineralization in the growth plate where accumulated p-OPN is exerting its inhibitory influence in *Phospho1*$^{-/-}$ mice.

We observed improved BV/TV, improved trabecular and cortical thickness, and reduced trabecular spaces and cortical porosity at 1 month of age in [*Phospho1*$^{-/-}$; *Spp1*$^{-/-}$] mice as is observed in the *Spp1*$^{-/-}$ mice. These data show that the bone phenotype of the [*Phospho1*$^{-/-}$; *Spp1*$^{-/-}$] mice displays intermediate severity compared with those of the individual *Spp1*$^{-/-}$ and *Phospho1*$^{-/-}$ phenotypes. Cortical BMD of both tibia and femur was

also improved in the [*Phospho1*$^{-/-}$; *Spp1*$^{-/-}$] mice at 1 month of age. At 3 months of age, the *Phospho1*$^{-/-}$ mice did not show any significant difference in BMD from the WT mice. This could be because of increased bone at the sites of callus formation during fracture healing. The improved phenotype of the [*Phospho1*$^{-/-}$; *Spp1*$^{-/-}$] mice can be explained by the significant changes in gene expression that result in promineralizing conditions in [*Phospho1*$^{-/-}$; *Spp1*$^{-/-}$] cells, such as the normalization of the calcifying ability of [*Phospho1*$^{-/-}$; *Spp1*$^{-/-}$] chondrocytes, the increase in *Alpl* expression in these cells, and the increase in plasma TNAP activity in the double knockout mice, which results in normalized plasma PP_i concentrations. Fig. 7 helps visualize how removing the regulatory influences exerted by PHOSPHO1 and OPN would only leave a functional P_i/PP_i pathway to control mineralization in [*Phospho1*$^{-/-}$; *Spp1*$^{-/-}$] cells and mice.

Supplementary Material

Refer to Web version on PubMed Central for supplementary material.

Acknowledgments

We thank the animal facility personnel and the histology and proteomics services at the Sanford-Burnham Medical Research Institute for their invaluable help. We also thank Mr John Shelly for cutting undecalcified plastic sections at the Sanford-Burnham Medical Research Institute (Lake Nona, FL, USA).

This work was funded by grant DE012889 from the National Institute of Dental and Craniofacial Research (NIDCR) and grant AR053102 from the National Institute of Arthritis and Musculoskeletal Diseases (NIAMS), National Institutes of Health, USA.

References

1. Stewart AJ, Roberts SJ, Seawright E, Davey MG, Fleming RH, Farquharson C. The presence of PHOSPHO1 in matrix vesicles and its developmental expression prior to skeletal mineralization. Bone. 2006; 39:1000–1007. [PubMed: 16837257]
2. Roberts S, Narisawa S, Harmey D, Millán JL, Farquharson C. Functional involvement of PHOSPHO1 in matrix vesicle-mediated skeletal mineralization. J Bone Miner Res. 2007; 22:617–627. [PubMed: 17227223]
3. Yadav MC, Simao AMS, Narisawa S, et al. Loss of skeletal mineralization by the simultaneous ablation of PHOSPHO1 and alkaline phosphatase function: a unified model of the mechanisms of initiation of skeletal calcification. J Bone Miner Res. 2011; 26:286–297. [PubMed: 20684022]
4. Huesa C, Yadav MC, Finnila MAJ, et al. PHOSPHO1 is essential for mechanically competent mineralization and the avoidance of spontaneous fractures. Bone. 2011; 48:1066–1077. [PubMed: 21272676]
5. McKee MD, Yadav MC, Foster BL, Somerman MJ, Farquharson C, Millán JL. Compounded PHOSPHO1/ALPL deficiencies reduce dentin mineralization. J Dent Res. 2013; 92:721–727. [PubMed: 23694930]
6. Millán JL. The role of phosphatases in the initiation of skeletal mineralization. Calcif Tissue Int. 2013; 93:299–306. [PubMed: 23183786]
7. Murshed M, Harmey D, Millán JL, McKee MD, Karsenty G. Unique coexpression in osteoblasts of broadly expressed genes accounts for the spatial restriction of ECM mineralization to bone. Genes Dev. 2005; 19:1093–1104. [PubMed: 15833911]
8. Millán JL, Narisawa S, Lemire I, et al. Enzyme replacement therapy for murine hypophosphatasia. J Bone Miner Res. 2008; 23:777–787. [PubMed: 18086009]

9. Boskey AL, Maresca M, Ulrich W, Doty SB, Butler WT, Prince CW. Osteopontin hydroxyapatite interactions in vitro. Inhibition of hydroxyapatite formation and growth in a gelatin gel. Bone Miner. 1993; 22:147–159. [PubMed: 8251766]
10. Hunter GK, Kyle CL, Goldberg HA. Modulation of crystal formation by bone phosphoproteins; structural specificity of the osteopontin-mediated inhibition of hydroxyapatite formation. Biochem J. 1994; 300:723–728. [PubMed: 8010953]
11. Sodek J, Ganss B, McKee MD. Osteopontin. Crit Rev Oral Biol Med. 2000; 11:279–303. [PubMed: 11021631]
12. Hunter GK. Role of osteopontin in modulation of hydroxyapatite formation. Calcif Tissue Int. 2013; 93:348–354. [PubMed: 23334303]
13. Oldberg A, Franzen A, Heinegard D. Cloning and sequence analysis of rat bone sialoprotein (osteopontin) cDNA reveals an Arg-Gly-Asp cell-binding sequence. Proc Natl Acad Sci USA. 1986; 83:8819–8823. [PubMed: 3024151]
14. Sorensen ES, Hojrup P, Petersen TE. Posttranslational modifications of bovine osteopontin: identification of twenty-eight phosphorylation and three O-glycosylation sites. Protein Sci. 1995; 4:2040–2049. [PubMed: 8535240]
15. Addison WN, Masica DL, Gray JJ, McKee MD. Phosphorylation-dependent inhibition of mineralization by osteopontin ASARM peptides is regulated by PHEX cleavage. J Bone Miner Res. 2010; 25:695–705. [PubMed: 19775205]
16. Boskey AL, Spevak L, Paschalis E, Doty SB, McKee MD. Osteopontin deficiency increases mineral content and mineral crystallinity in mouse bone. Calcif Tissue Int. 2002; 71:145–154. [PubMed: 12073157]
17. Harmey D, Hessle L, Narisawa S, Johnson KA, Terkeltaub R, Millán JL. Elevated skeletal osteopontin levels contribute to the hypophosphatasia phenotype in Akp2$^{-/-}$ mice. J Bone Miner Res. 2006; 21:1377–1386. [PubMed: 16939396]
18. Johnson K, Goding J, Van Etten D, et al. Linked deficiencies in extracellular PPi and osteopontin mediate pathologic calcification associated with defective PC-1 and ANK expression. J Bone Miner Res. 2003; 18:994–1004. [PubMed: 12817751]
19. Harmey D, Hessle L, Narisawa S, Johnson KA, Terkeltaub R, Millán JL. Concerted regulation of inorganic pyrophosphate and osteopontin by Akp2, Enpp1, and Ank—an integrated model of the pathogenesis of mineralization disorders. Am J Pathol. 2004; 164:1199–1209. [PubMed: 15039209]
20. Addison WN, Azari F, Sorensen ES, Kaartinen MT, McKee MD. Pyrophosphate inhibits mineralization of osteoblast cultures by binding to mineral, up-regulating osteopontin and inhibiting alkaline phosphatase activity. J Biol Chem. 2007; 282:15872–15883. [PubMed: 17383965]
21. Rittling SR, Matsumoto HN, McKee MD, et al. Mice lacking osteopontin show normal development and bone structure but display altered osteoclast formation in vitro. J Bone Miner Res. 1998; 13:1101–1111. [PubMed: 9661074]
22. Narisawa S, Wennberg S, Millán JL. Abnormal vitamin B6 metabolism in alkaline phosphatase knock-out mice causes multiple abnormalities, but not the impaired bone mineralization. J Pathol. 2001; 193:125–133. [PubMed: 11169525]
23. Hessle L, Johnson KA, Anderson HC, et al. Tissue-nonspecific alkaline phosphatase and plasma cell membrane glycoprotein-1 are central antagonistic regulators of bone mineralization. Proc Natl Acad Sci USA. 2002; 99:9445–9449. [PubMed: 12082181]
24. Prince CW, Oosawa T, Butler WT, et al. Isolation, characterization, and biosynthesis of phosphorylated glycoprotein from rat bone. J Biol Chem. 1987; 262:2900–2907. [PubMed: 3469201]
25. Narisawa S, Yadav MC, Millán JL. In vivo overexpression of tissue-nonspecific alkaline phosphatase increases skeletal mineralization and affects the phosphorylation status of osteopontin. J Bone Miner Res. 2013; 28:1587–1598. [PubMed: 23427088]
26. Moreau, A., Franco, A., Azeddine, B., et al. High circulating levels of osteopontin are associated with idiopathic scoliosis onset and spinal deformity progression. Presented at: 44th Annual Meeting Scoliosis Research Society; September 23–26, 2009; San Antonio, TX, USA.

27. Steitz SA, Speer MY, McKee MD, et al. Osteopontin inhibits mineral deposition and promotes regression of ectopic calcification. Am J Pathol. 2002; 161:2035–2046. [PubMed: 12466120]
28. Mo L, Liaw L, Evan AP, Sommer AJ, Lieske JC, Wu XR. Renal calcinosis and stone formation in mice lacking osteopontin, Tamm-Horsfall protein, or both. Am J Physiol Renal Physiol. 2007; 293:F1935–F1943. [PubMed: 17898038]
29. Speer MY, McKee MD, Guldberg RE, et al. Inactivation of the osteopontin gene enhances vascular calcification of matrix Gla protein–deficient mice: evidence for osteopontin as an inducible inhibitor of vascular calcification in vivo. J Exp Med. 2002; 196:1047–1055. [PubMed: 12391016]
30. Wesson JA, Johnson RJ, Mazzali M, et al. Osteopontin is a critical inhibitor of calcium oxalate crystal formation and retention in renal tubules. J Am Soc Nephrol. 2003; 14:139–147. [PubMed: 12506146]
31. Shapses SA, Cifuentes M, Spevak L, et al. Osteopontin facilitates bone resorption, decreasing bone mineral crystallinity and content during calcium deficiency. Calc Tissue Int. 2003; 73:86–92.
32. Rittling SR, Denhardt DT. Osteopontin function in pathology: lessons from osteopontin deficient mice. Exp Nephrol. 1999; 7:103–113. [PubMed: 10213864]
33. Liu YK, Uemura T, Nemoto A, et al. Osteopontin involvement in integrin-mediated cell signaling and regulation of expression of alkaline phosphatase during early differentiation of UMR cells. FEBS Lett. 1997; 420:112–116. [PubMed: 9450560]
34. Polewski MD, Johnson KA, Foster M, Millán JL, Terkeltaub R. Inorganic pyrophosphatase induces type I collagen in osteoblasts. Bone. 2010; 46:81–90. [PubMed: 19733704]
35. Whyte MP, Valdes R Jr, Ryan LM, McAlister WH. Infantile hypophosphatasia: enzyme replacement therapy by intravenous infusion of alkaline phosphatase-rich plasma from patients with Paget bone disease. J Pediatr. 1982; 101:379–386. [PubMed: 7108657]
36. Whyte MP, McAlister WH, Patton LS, et al. Enzyme replacement therapy for i nfantile hypophosphatasia attempted by intravenous infusions of alkaline phosphatase-rich Paget plasma: results in three additional patients. J Pediatr. 1984; 105:926–933. [PubMed: 6502342]
37. Whyte MP, Greenberg CR, et al. Enzyme- replacement therapy in life threatening hypophosphatasia. N Engl J Med. 2012; 366(10):904–913. [PubMed: 22397652]

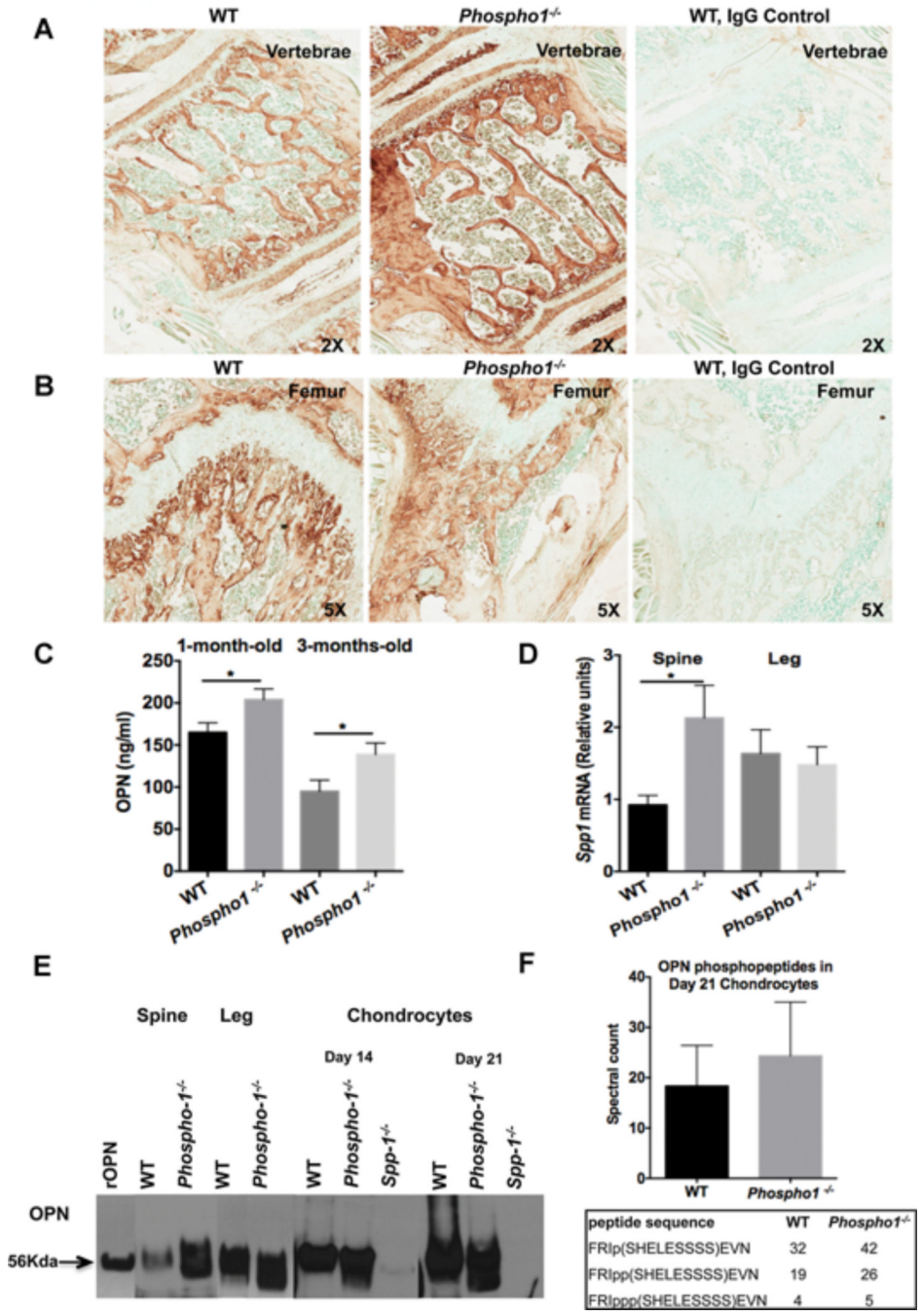

Figure 1.

Expression of OPN in the spine and plasma of *Phospho1*$^{-/-}$ mice is higher than in WT mice. Immunohistochemistry using anti-OPN antibody on the vertebral body (*A*) and femur (*B*) from WT and *Phospho1*$^{-/-}$ mice shows higher expression of OPN in the spine of *Phospho1*$^{-/-}$ mice than in WT mice. No changes in OPN expression were observed between the femur of *Phospho1*$^{-/-}$ and WT mice. Negative control with normal goat IgG in WT mice (*A, B*) shows no OPN signal. Images are representative of three individual mice. (*C*) OPN ELISA also shows higher OPN levels in the plasma of both 1- and 3-month-old *Phospho1*$^{-/-}$

mice than in WT mice ($n \geq 7$ mice per group). (*D*) RNA expression data show higher *Spp1* gene expression in the spine of *Phospho1*$^{-/-}$ mice than in WT, whereas no changes are observed in the femur ($n = 3$). (*E*) Western blot using anti-OPN antibody showing OPN levels in femur, spine, and day 14 and day 21 cultured chondrocytes from WT and *Phospho1*$^{-/-}$ mice. The 56-kDa band represents mouse recombinant OPN. (*F*) Mass spectrometry analysis of protein extracts from cultured chondrocytes from WT and *Phospho1*$^{-/-}$ mice immunoprecipitated with anti-OPN antibody. Residue numbers are based on the OPN isoform NP_001191131. The spectral counts of individual phosphopeptides show greater numbers of phosphorylated OPN sequences in *Phospho1*$^{-/-}$ mice than in WT mice.

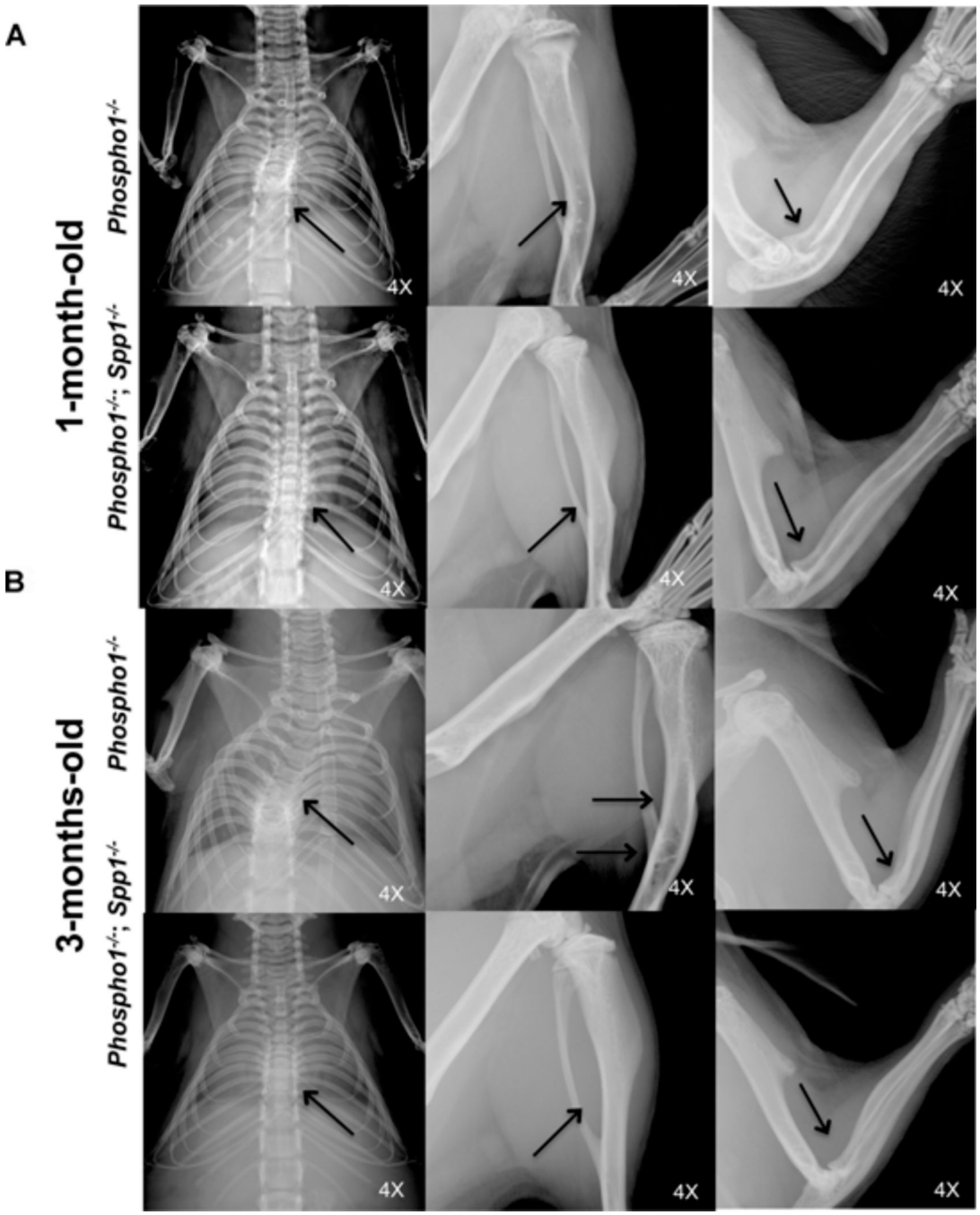

Figure 2.

Improvement of the scoliosis and other skeletal abnormalities in [*Phospho1*$^{-/-}$; *Spp1*$^{-/-}$] mice. (*A, B*) Radiographic images of *Phospho1*$^{-/-}$ and [*Phospho1*$^{-/-}$; *Spp1*$^{-/-}$] mice at 1 and 3 months of age. (*A*) [*Phospho1*$^{-/-}$; *Spp1*$^{-/-}$] mice showed slightly less scoliosis than *Phospho1*$^{-/-}$ mice at 1 month of age (arrows) but no change in the long bone abnormalities. (*B*) No scoliosis was observed at 3 months of age in [*Phospho1*$^{-/-}$; *Spp1*$^{-/-}$] mice (arrows). Less bowing of long bones and no fractures (in the tibias) are observed in [*Phospho1*$^{-/-}$; *Spp1*$^{-/-}$] mice than in *Phospho1*$^{-/-}$ mice. Images are representative of at least three

individual mice for each genotype. Arrows show bowed long bones and fractures in the tibias in *Phospho1*$^{-/-}$ mice.

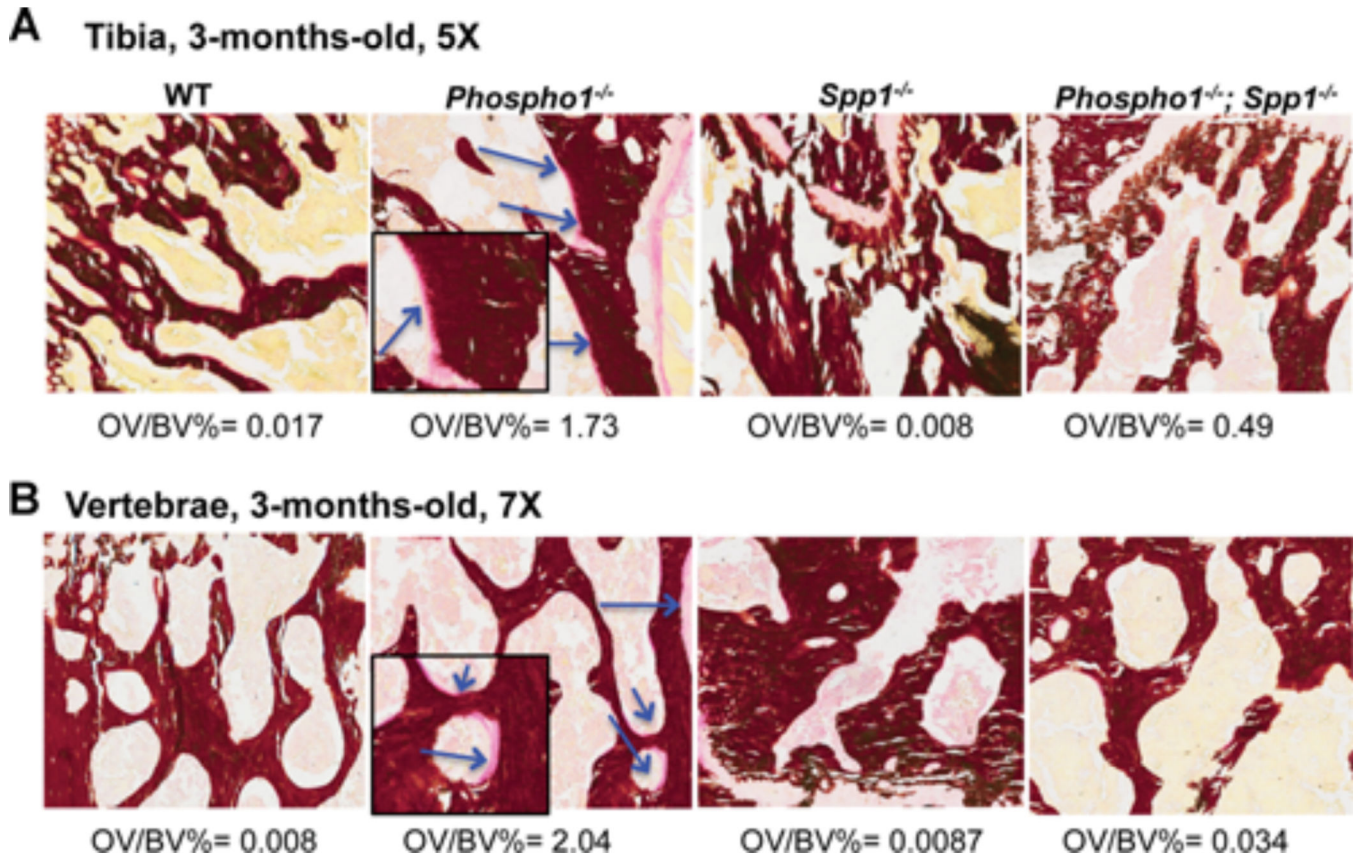

Figure 3.

Histomorphometric analyses of tibias (*A*) and spines (*B*) of WT, *Phospho1*$^{-/-}$, *Spp1*$^{-/-}$, and [*Phospho1*$^{-/-}$; *Spp1*$^{-/-}$] mice at 3 months of age. Von Kossa/van Gieson staining of the tibial section at the knee joint reveals trabecular bone surrounded by widespread, extended osteoid in 3-month-old *Phospho1*$^{-/-}$ mice (arrows/inserts show higher magnification of the areas where the osteoid is present), which is less apparent in [*Phospho1*$^{-/-}$; *Spp1*$^{-/-}$] mice.

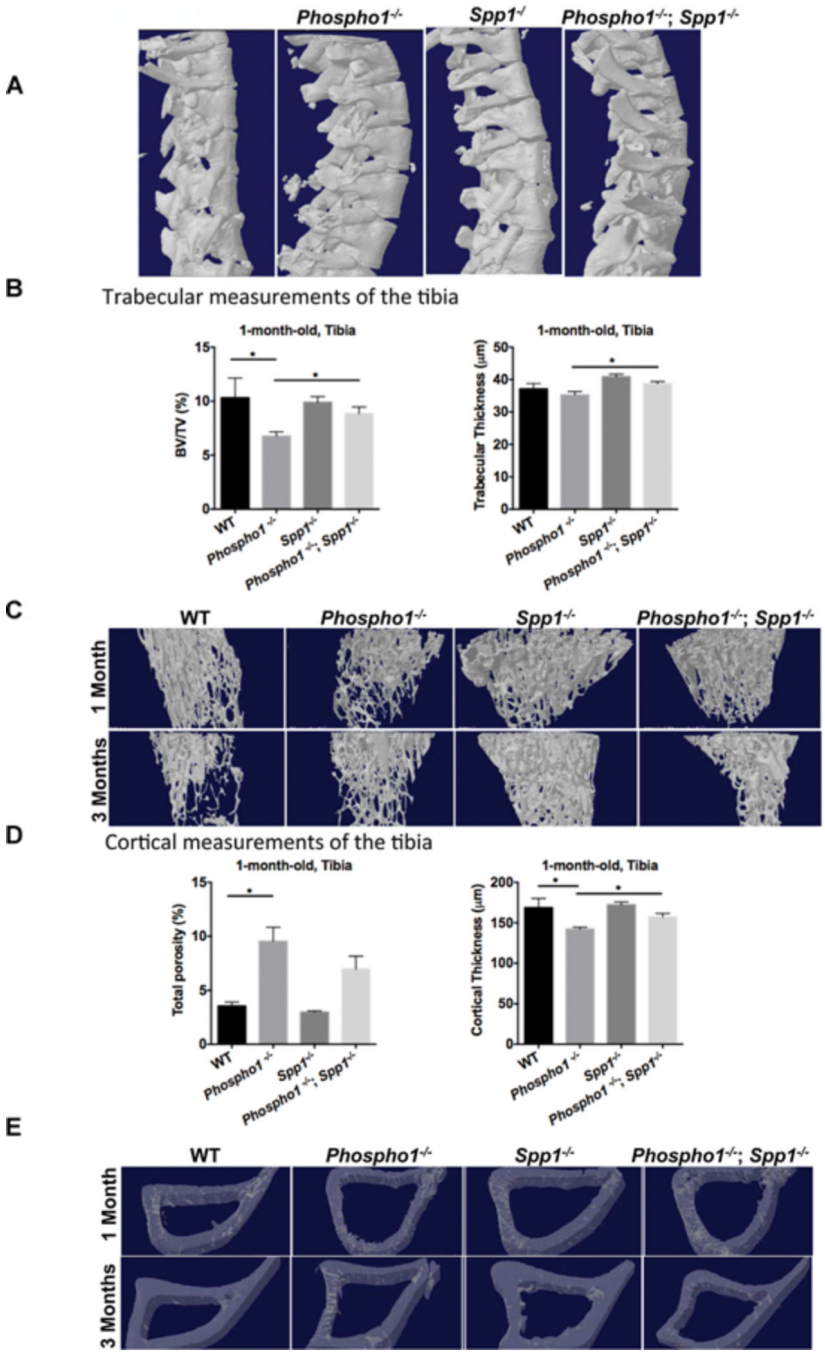

Figure 4.

μCT analysis of spine and tibia in WT, *Phospho1*$^{-/-}$, *Spp1*$^{-/-}$, and [*Phospho1*$^{-/-}$; *Spp1*$^{-/-}$] mice. (*A*) 3D reconstructions of the thoracic vertebrae at 3 months of age from μCT scans at a resolution of 10 μm. (*B*) The ratio of bone volume to the selected area of trabecular bone (BV/TV), expressed as a percentage, and trabecular thickness in 1-month-old mice. (*C*) Representative 3D models of trabecular bone showing greater trabecular thickness and smaller trabecular spaces in the [*Phospho1*$^{-/-}$; *Spp1*$^{-/-}$] mice. (*D*) Total cortical porosity and thickness in 1-month-old mice. (*E*) Representative 3D models of cortical bone showing

greater cortical thickness in the [*Phospho1*$^{-/-}$; *Spp1*$^{-/-}$] mice. The bone has been made transparent to be able to see the porosity/vascularity. *$p < 0.05$, **$p < 0.01$.

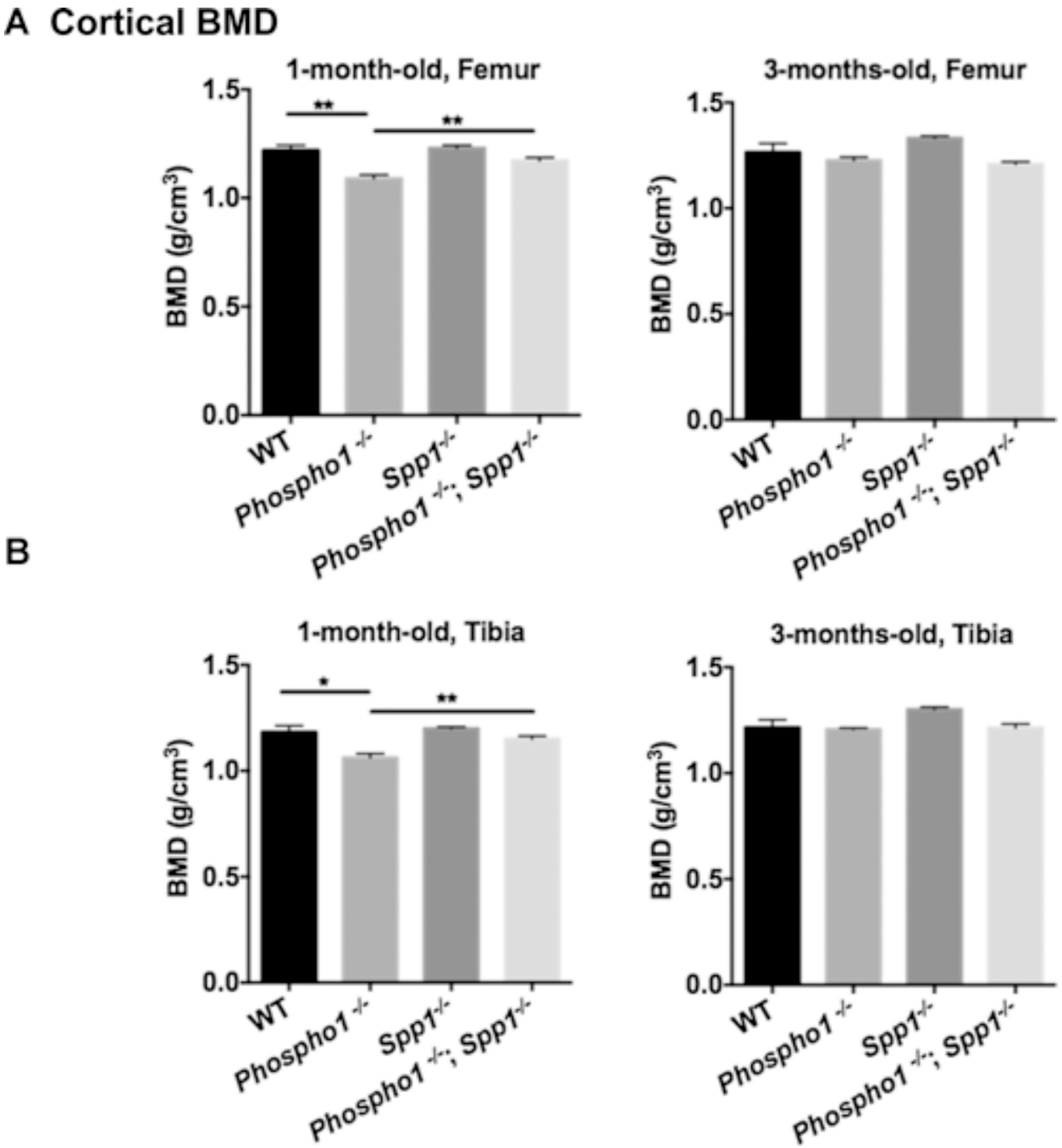

Figure 5.

Bone mineral density analysis by μCT in WT, *Phospho1*$^{-/-}$, *Spp1*$^{-/-}$, and [*Phospho1*$^{-/-}$; *Spp1*$^{-/-}$] mice. Cortical bone mineral density analysis of femur (*A*) and tibia (*B*) of 1-month- and 3-monthold mice shows no difference in the BMD of WT and *Spp1*$^{-/-}$ mice both at either age. At 1 month of age, *Phospho1*$^{-/-}$ mice show lower BMD, which was not observed in *Phospho1*$^{-/-}$; *Spp1*$^{-/-}$ mice. $n \geq 3$, *$p < 0.05$, **$p < 0.01$.

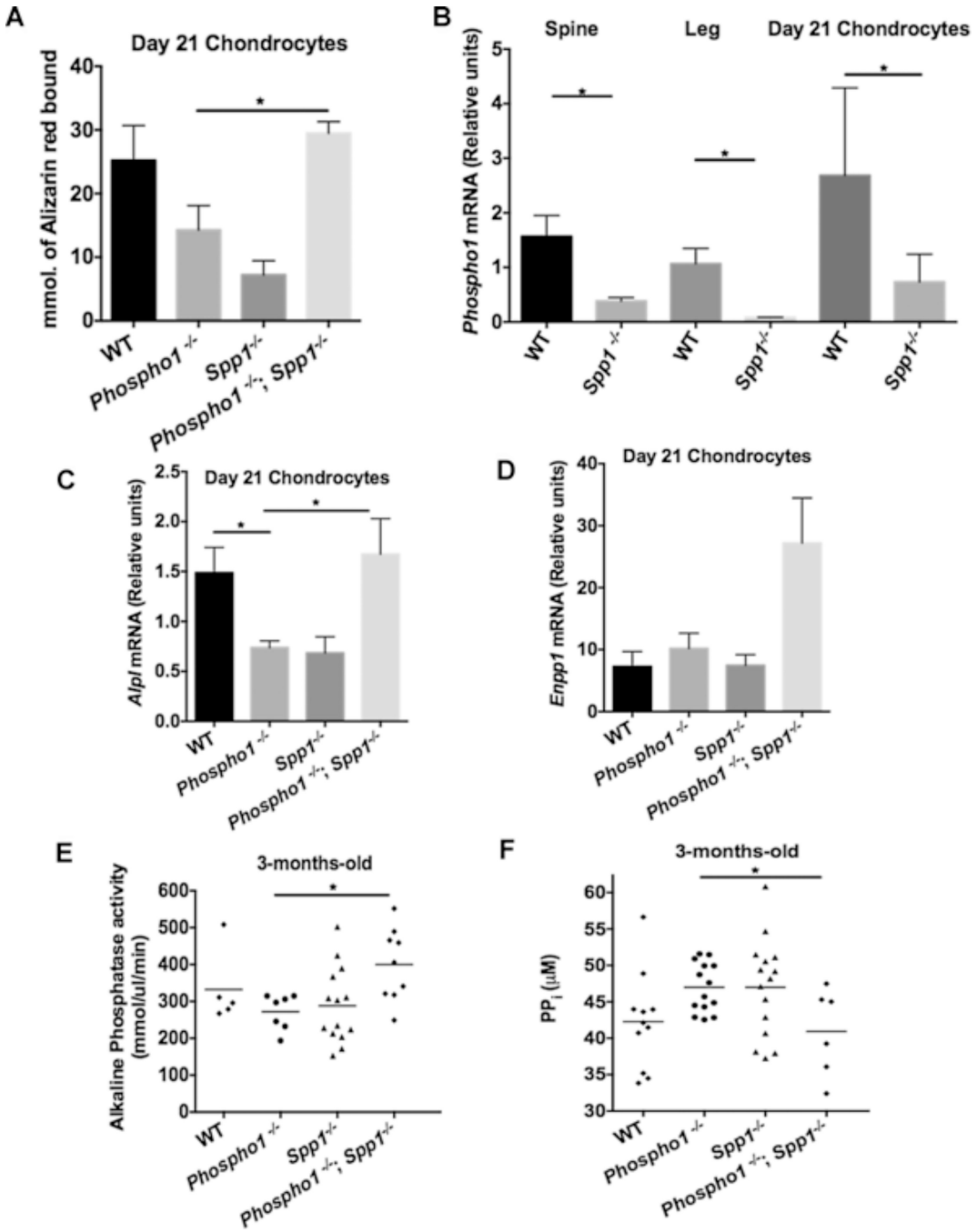

Figure 6.

Chondrocyte mineralization and plasma analysis in WT, *Phospho1*$^{-/-}$, *Spp1*$^{-/-}$, and [*Phospho1*$^{-/-}$; *Spp1*$^{-/-}$] mice. (*A*) Chondrocyte mineralization assay using Alizarin red staining at days 14 and 21 of culture also showed improved mineralization in the [*Phospho1*$^{-/-}$; *Spp1*$^{-/-}$] mice compared with *Phospho1*$^{-/-}$ mice alone. (*B*) *Phospho1* gene expression was reduced in spine, leg, and 21-day cultured chondrocytes of *Spp1*$^{-/-}$ mice ($n \geq 3$). Data are represented as mean ± SEM, experiments done in triplicates. (*C*) *Alpl* expression in 21-day chondrocyte cultures. *Phospho1*$^{-/-}$ mice show reduced *Alpl* gene

expression, which was significantly increased in [*Phospho1*$^{-/-}$; *Spp1*$^{-/-}$] mice. (*D*) *Enpp1* in 21-day chondrocyte cultures. *Enpp1* expression was slightly increased in *Phospho1*$^{-/-}$ mice and significantly increased in the [*Phospho1*$^{-/-}$; *Spp1*$^{-/-}$] mice. $n \geq 3$, experiments performed in duplicate. TNAP activity (*E*) and PP_i concentration (*F*) in plasma of 3-month-old mice. TNAP levels were higher and PP_i levels were lower in the plasma of [*Phospho1*$^{-/-}$; *Spp1*$^{-/-}$] mice than in *Phospho1*$^{-/-}$ mice. Data are represented as mean ± SEM, $n \geq 6$ mice per group, experiments performed in duplicate.

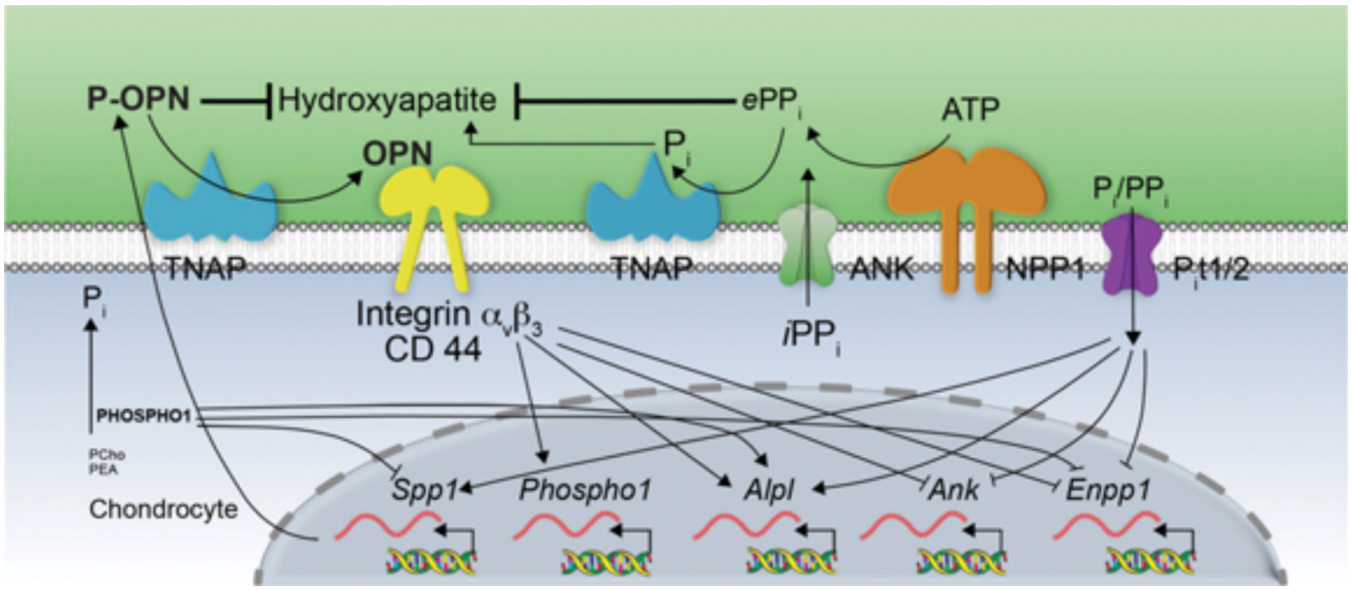

Figure 7.

Schematic model showing the counter-regulatory influences exerted by the P_i/PP_i ratio, OPN, and PHOSPHO1 on mineralizing cells.